Geophysical Research Letters

Supporting Information for

How obliquity cycles powered early Pleistocene global ice-volume variability

Clay R. Tabor[1], Christopher J. Poulsen[1], David Pollard[2]

1. Department of Earth and Environmental Sciences, University of Michigan, Ann Arbor, Michigan, USA.

2. Earth and Environmental Systems Institute, Pennsylvania State University, University Park, Pennsylvania, USA.

Contents of this file

Introduction

This auxiliary material provided here are additional model configuration details (text S1), the individual standardized power spectra of the ice-volume responses (figure S1), decomposed seasonal offsets (figure S2), the relationships between ice and ablation (figure S3), the additional run cycle from OC2 (figure S4), and a table of the four orbital configurations used in this study (table S1).

Text S1.

Additional experiment design details

In our ice sheet experiments, we used an insolation/temperature melt scheme. The melt, M, is calculated with the following equation:

$$M = \Delta t\,[\mathcal{T}(1-\alpha)Q + c + 10T]/(1000L_m) \quad \text{(S1)}$$

where M is the melt in meters, Δt is a day in seconds, α is the albedo, $\mathcal{T}$ is the transmissivity of the atmosphere, T is the lowest atmospheric layer temperature in °C, Q is the daily insolation at the top of the atmosphere in W m^{-2}, L_m is the latent heat of melting in J kg^{-1}, and c is a constant equal to -100 based on our modern day model experiments. Here α, $\mathcal{T}$, Q, and T, are taken from the daily GCM outputs.

The asynchronous coupling technique that allows us to capture the transient climate response to long-term orbital changes involves running the GCM with a fixed orbital configuration for 25 yr. The final 10 yr of the GCM integration are averaged and passed to the ice-sheet model to calculate surface mass balance. After forcing the ice-sheet model for 2.5 kyr with the GCM outputs, updated land surface type and topography data are fed back into the GCM along with an appropriately advanced orbital configuration [*Pollard et al.*, 1990]. Because orbits with large eccentricity alter seasonal duration, we use an angular calendar for all monthly and seasonal comparisons following Joussaume and Braconnot [1997]. Each month in our angular calendar corresponds with 30° arc length of Earth's orbit around the Sun.

For the climate-ice experiments, we run two orbital cycles, equivalent to 80 kyr. The ice-sheets require a cycle to equilibrate; therefore, the first cycle is removed from our analysis. We confirm that the ice-volume signals are producing consistent cycle responses by running the OC4 orbital configuration for an additional orbital cycle (40 kyr) (Figure S4) and find virtually no difference in the ice-volume response between the 40-80 kyr and 80-120 kyr cycles. Given consistent cycles, we combine several of the same ice-volume cycles together to calculate the

ice-volume power spectra.

No floating ice or grounding-line advance into water is allowed in the ice-sheet model. Because the Scandinavian ice sheet contains a large shelf component, we limit our ice domain to North America and Greenland. In order for ice to advance onto the continental shelf and over the Hudson Bay, we lower sea level by 275 m in this region in the ice-sheet model relative to modern day. Our artificial sea level reduction might be justified since there is no evidence that the Hudson Bay was below sea level during the Pliocene [*Sohl et al.*, 2009]. Additionally, due to the inability of the AGCM to capture valley ablation in Alaska [*Marshall and Clarke*, 1999], a 6°C temperature bias correction is applied to the region when running the ice-sheet model to prevent permanent ice build up. The temperature adjustment only applies to the ice sheet model component, not the GCM, and therefore, has no impact on the climate-only experiments. Furthermore, previous tests suggest that the temperature bias correction does not significantly change the pattern of our ice sheet response.

References

Joussaume, S., and P. Braconnot (1997), Sensitivity of paleoclimate simulation results to season definitions, *J. Geophys. Res.*, *102*(D2), 1943-1956, doi:10.1029/96JD01989.

Marshall, S. J., and G. Clarke (1999), Modeling North American freshwater runoff through the last glacial cycle, *Quat. Res.*, *52*(3), 300–315, doi:10.1006/qres.1999.2079.

Pollard, D., I. Muszynski, S. H. Schneider, and S. L. Thompson (1990), Asynchronous coupling of ice sheet and atmospheric forcing models, *Ann. Glac.*, 6, 255-272, doi:10.5194/tc-6-255-2012.

Sohl, L.E., M.A. Chandler, R.B. Schmunk, K. Mankoff, J.A. Jonas, K.M. Foley, and H.J. Dowsett (2009), PRISM3/GISS topographic reconstruction. *USGS.*

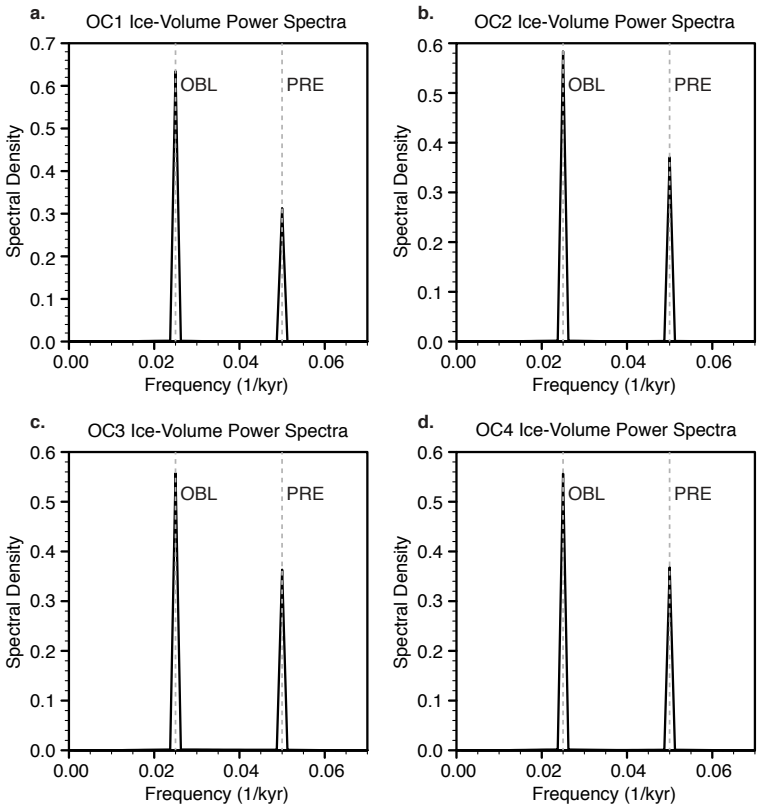

Figure S1. The individual standardized power spectra of the ice-volume response to the four transient orbital configurations. (a-d) Power spectra plots for orbital configurations OC1-4. While there is a bit of variability in frequency power distribution between orbital configurations, the obliquity frequency produces a stronger ice-volume signal than precession for all orbital configurations. Vertical dashed gray lines highlight the location of the obliquity and precession frequencies.

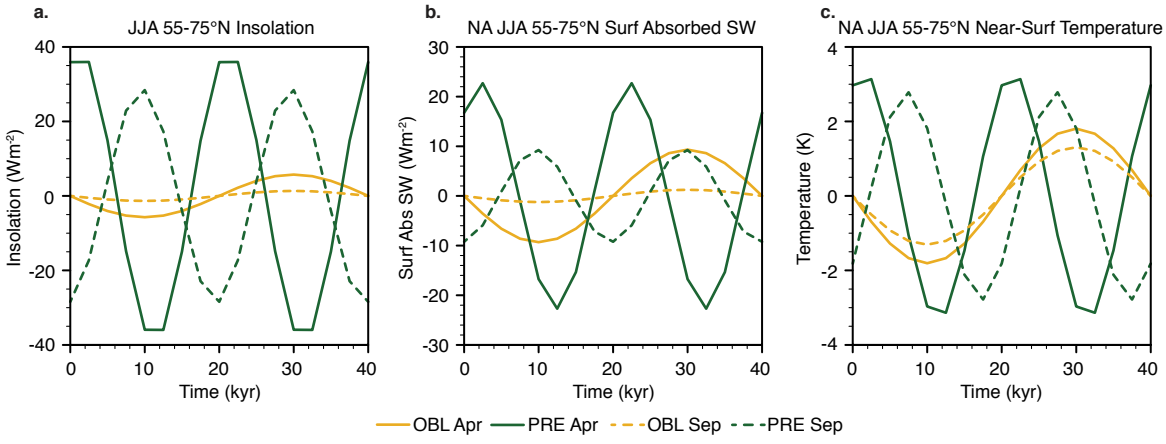

Figure S2. Decomposition of NA HL April and September signals into obliquity and precession components. Spatial and temporal averages of NA HL (55-75°N, 57-165°W) April (solid lines) and September (dashed lines) signals are decomposed into obliquity (oranges lines) and precession (green lines) components to highlight the seasonal differences in insolation forcing and climate response. Plots show the differences in insolation forcing between obliquity and precession over 40 kyr, equivalent to one obliquity cycle and two precession cycles. (a) The insolation (W m^{-2}) contributions from obliquity and precession for April and September. (b) The surface-absorbed shortwave radiation (W m^{-2}) contributions from obliquity and precession for April and September. (c) The near-surface temperature (K) contributions from obliquity and precession for April and September. These plots show that the in-phase seasonal forcing of obliquity amplifies absorbed shortwave radiation and near-surface temperature responses while the out-of-phase seasonal precession forcing leads to some offset in the same responses.

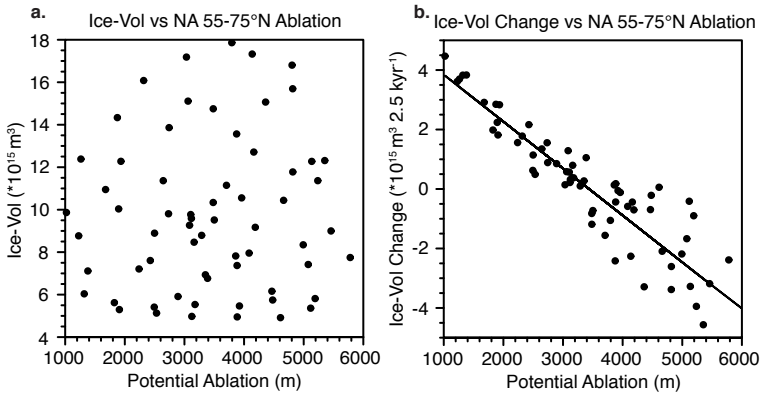

Figure S3. The relationships between ice and ablation. (a) Ice-volume (m^3) on the y axis is plotted against average NA HL (55-75°N, 57-165°W) potential ablation (m) over land from the climate-only experiments on the x axis. There is no correlation between ice-volume and ablation. (b) Ice-volume change on the y axis is plotted against potential ablation (m) over land from the climate-only experiments on the x axis. There is a strong linear relationship between the change

in ice-volume and NA HL ablation, suggesting the model ice-volume is mainly in response to changes in ablation.

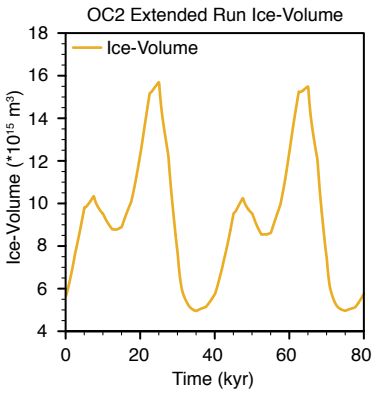

Figure S4. OC2 was run for an additional orbital cycle to show that the differences in the ice-volume (m^3) response between cycles are minimal. The ice-volume response over the first 40 kyr is nearly identical to the second 40 kyr and shows almost no difference in spectral power.

Orbital configurations

	Starting Precession	Starting Obliquity	Eccentricity
OC1	0°	23.3085°	0.056596
OC2	90°	23.3085°	0.056596
OC3	180°	23.3085°	0.056596
OC4	270°	23.3085°	0.056596

Table S1. The starting values of precession, obliquity, and eccentricity for the four transient orbital configurations. The only difference between orbital configurations is the phasing of precession relative to obliquity. Obliquity ranges from 22.079 to 24.538°, precession includes 360° cycles representing the prograde angle from perihelion to NH Vernal Equinox, and eccentricity is held constant at 0.056596. Both the obliquity range and eccentricity represent the extremes of the Pleistocene.